Journal of Environmental Chemical Engineering 11 (2023) 109171

Contents lists available at ScienceDirect

Journal of Environmental Chemical Engineering

journal homepage: www.elsevier.com/locate/jece

Coupling continuous CO_2 electroreduction to formate with efficient Ni-based anodes

Guillermo Díaz-Sainz [a,*], Kevin Fernández-Caso [a], Tiago Lagarteira [b], Sofia Delgado [b], Manuel Alvarez-Guerra [a], Adélio Mendes [b], Angel Irabien [a]

[a] Departamento de Ingenierías Química y Biomolecular, Universidad de Cantabria, ETSIIyT, Avenida de Los Castros s/n, 39005 Santander, Spain
[b] Laboratory for Process Engineering, Environmental, Biotechnology and Energy (LEPABE), University of Porto, Rua Dr. Roberto Frias S/n, Porto 4200-465, Portugal

ARTICLE INFO

Editor: Dr. Zhang Xiwang

Keywords:
Electrocatalytic CO_2 reduction
Formate
NiO catalyst
Counter electrodes
Oxygen evolution reaction

ABSTRACT

CO_2 electroreduction to formic acid and formate has been focus of great research attention in the last years. Thus, considerable and relevant efforts have been accomplished in this field, mainly by operating with different types of catalysts and electrode configurations in the cathodic compartment. Still, Pt-based anodes, which are expensive and scarce, are typically the preferred materials to carry out the oxygen evolution reaction in alkaline medium. However, it is crucial to search for new materials of lower prices, with high stability, and good performances able to be competitive with traditional Pt-based electrodes. Hence, we study hand-made NiO-based anodes for the continuous CO_2 electroreduction for formate in a filter press reactor with a single pass of the reactants through the electrochemical reactor. The use of the NiO-based anodes enhances the results obtained in previous studies with DSA/O_2 anodes, combining excellent values of Faradaic Efficiency for formate of 100 %, and energy consumptions values close to only 200 kWh·kmol^{-1}. In addition, employing Sustainion® as a binder in the fabrication of the anode results in a significant improvement in the durability, maintaining similar performance in terms of key metrics.

1. Introduction

The World Meteorological Organization (WMO) has recently announced that the concentration of carbon dioxide (CO_2) has reached 415.7 parts per million in 2021, which is 149 points in percentage higher than the pre-industrial level [1]. Moreover, one of the goals proposed for the UN Climate Change Conference of the Parties (COP27) hosted in Sharm El Sheikh (Egypt) is to limit the temperature increase to 1.5 ºC above pre-industrial levels [2]. This is why the electrocatalytic reduction of CO_2 into chemicals with value-added driven by electrical renewable energy is gaining attention and appears as a promising strategy to mitigate climate change [3–5]. Among the different products that can be obtained from CO_2 reduction, formate is considered a widely used chemical commodity in different pharmaceutical or leather industries [6,7]. Besides, formate can be supplied as fuel (starting from 0.5 M in solution) for direct formate fuel cells (DFAFCs) to produce electricity, and it is considered one of the highest value-added CO_2 conversion products in terms of market price since this chemical reaches a value of around $1000 - $1700 per ton of product [8].

Over the last few years, great efforts and huge progress have been made to accomplish formic acid and formate from CO_2 electroreduction by studying mainly (i) diverse cathode materials [9–11], (ii) several types of electrodes and reactors configurations [12–14], and (iii) environmental and economic analysis of this electrochemical process [15–17]. Specifically, research efforts have been focused so far on the cathodic compartment emphasizing the use of Sn [18–21], Bi [22–25], In [26,27], Sb [28], and Pb-based materials [29] as electrocatalysts used in different electrode configurations, such as metallic plate [30–32], Gas Diffusion Electrode (GDE) [33–35], and Catalyst Coated Membrane Electrode (CCME) [36–38], where CO_2 is converted into value-added products, and particularly to formic acid and formate.

While CO_2 is reduced at the cathode side, an oxidation must occur at the anode side, which can influence the performance of the desired reaction, so the nature and configuration of the catalyst used for that oxidation in the anode have an influence on the reduction semireaction to which is linked. In this sense, the majority of these research works have studied the electrochemical conversion of CO_2 towards formic acid or formate with anodes where oxygen evolution reaction (OER) (i.e.

* Corresponding author.
E-mail address: diazsg@unican.es (G. Díaz-Sainz).

https://doi.org/10.1016/j.jece.2022.109171
Received 2 November 2022; Received in revised form 9 December 2022; Accepted 13 December 2022
Available online 16 December 2022

oxidation of water to give molecular oxygen) takes place, using mainly noble metal catalysts, such as Pt and Ir (or IrO_2) based-materials to shape the counter electrode in the form of gauze [39], foil [40], plate [41], wire [42], metallic plate [43] or particulate electrode, especially in acidic media [44]. In this sense, these metals are the most active materials in a wide range of pH, but their high price and limited supply strain the researchers to find non-precious alternatives for the large-scale industrial implementation [45–47].

Thus, there are recent works employing alternative, precious group metal (PGM)-free based materials, and particularly the first-row transition metals, to carry out the OER in the anodic compartment and simultaneously, the CO_2 electroreduction to value-added products in the cathodic compartment [48,49]. In particular, Ni-based catalysts have been suggested as promising alternative materials in the application of water splitting devices due to their low prices, abundant reserves, and great OER activities [50,51].

Ni-based materials could be considered as interesting electrocatalysts to carry out the OER in the counter electrode in processes for the electrocatalytic reduction of CO_2 towards formic acid and formate. In this sense, several manuscripts have recently focused on the CO_2 electroreduction to generate the approached target products by employing Ni materials for the OER [26,52–66]. A cheap, zero-gap electrochemical reactor, able to withstand wire range of differential partial pressures and to provide dynamic operation is the most anticipated configuration to bring the CO_2 electroreduction process closer to industrial applications [67]. In this way, Table 1 collects all the studies reported up to date in the literature, their characteristics, as well as the main figures of merit obtained which are reported in the field of CO_2 electroreduction to formic acid and formate working with Ni-based materials in the counter electrode in a continuous electrochemical reactor.

In particular, these studies employed mainly Ni in the form of commercial foams [26,52–62], mesh [63], gauzes [64], and foams of different alloys [56] as anodes for the OER. In this sense, to enhance the performance of the counter electrodes with respect to configurations employed up to date (i.e. foams, meshes, and gauzes), further efforts are needed in the development and fabrication of new Ni-based electrode configurations. Thus, and in line with the recent literature published in the field of the development of cathodes for the electrocatalytic reduction of CO_2 to formic acid and formate, the use of particulate electrodes or GDEs as anodes for generating oxygen over the counter electrode surface deserves further investigation. In fact, the main advantages of these configurations include higher active surface area of the electrocatalyst, and improved mass transport and electronic conduction to or from the external electrical circuit in comparison with conventional Ni-based electrodes [14].

In this context, here we report an assessment of Ni-based particulate anodes for the CO_2 electroreduction towards formate in a continuous filter press reactor with a single pass of the reactants through the electrochemical reactor. Firstly, the OER activity of diverse Ni-based materials was screened in a Rotating Disk Electrode set-up. Consequently, the material with the highest OER activity was chosen as the anodic electrocatalyst for subsequent tests of the continuous reduction of CO_2 to formate in a filter press reactor. These anodes were fabricated by the deposition of Ni-based catalysts by employing wet spray deposition. Besides, the influence of some key variables, such as the current density and the catholyte flow per geometric surface area on the performance of the process, was studied, achieving promising results in terms of formate concentration, Faradaic Efficiency, rate, and energy consumption. Subsequently, the results were improved, in comparison to those obtained previously using a commercial anode, by assessing the influence of variables in the anodic compartment (e.g. the anolyte concentration, and the anolyte flow per geometric surface area). Finally, the stability of the electrodes was enhanced by studying the influence of the binder in the fabrication of the anodes.

2. Methodology

2.1. Electrochemical characterization of Ni-based materials

The oxygen evolution reaction (OER) activity of different Ni-based materials was studied in a Rotating disk electrode (Autolab Rotating Disk Electrode, Metrohm Hispania) equipped with a potentiostat and impedance spectrometer (IM6-ex, ZAHNER-Elektrik). Two nickel oxide (NiO) commercial catalysts (Sigma-Aldrich) with different average particle sizes were tested for the OER. One of the NiO catalysts had an average particle size of 25 ± 10 nm (referred to as 1-NiO), while the size of the second catalyst was 50 nm (referred to as 2-NiO). The Ni-based electrode consisted of 5 mg of the catalyst deposited as a thin layer over a glassy carbon electrode (GCE) (0.196 cm^2). The inks were prepared by mixing the catalyst, 40 μL of Nafion™ solution (Nafion™ D-521, 5 % (w/w) in water/1-propanol, dispersion $\geq$ 0.92 meq·g^{-1} exchange, VWR), 2 mL of isopropanol (99.5 % Extradry, AcroSeal), and 8 mL of Milli-Q water (Millipore). Prior to each film deposition, the GCE was polished with a 0.05 mm alumina-particle solution. Consequently, the inks were sonicated in an ultrasonic bath (Selecta ultrasonic bath operating at 50/60 kHz, 360 power output) for 45 min to ensure a homogeneous mix. After sonication, two drops of 10 μL each were deposited on the GCE and dried at 700 rotations per minute (RPM) at room temperature. As a counter and reference electrode, a carbon rod and Ag/AgCl were employed, respectively. The electrolyte (1 M KOH, potassium hydroxide, 85 % purity, pharma grade, PanReac AppliChem)

Table 1
Summary of the experimental conditions and main results reported in literature for the electrocatalytic reduction of CO_2 to obtain formic acid or formate in a continuous mode of operation with Ni-based materials to carry out the OER in the working electrode.

Counter electrode	Anolyte	Current density (mA·cm^{-2})	Concentration of the target product (g·L^{-1})	Faradaic Efficiency (%)	Year	Reference
NiO particles	$KHCO_3$ 0.1 M	21	(-)	70	2022	[66]
Ni mesh	KOH 5 M	1800	(-)	70	2021	[63]
Ni foam	KOH 1 M	1000	1.30	93	2021	[55]
Ni foam	KOH 3 M	1000	(-)	93	2021	[26]
Fe/Ni foam	KOH 1 M	677	2.60	83	2021	[56]
Ni foam	KOH 1 M	570	0.36	91	2021	[59]
Ni foam	$KHCO_3$ 1 M	500	0.33	95	2021	[61]
Ni foam	KOH 1 M	258	(-)	92	2021	[60]
NiFe-LDHs-GDE	KOH 1 M	250	0.34	98	2021	[65]
NiFe LDH / Ni foam	KOH 1 M	160	(-)	74	2021	[58]
$Ni(OH)_2$ nanosheets on Ni foam	KOH (1.0 M) + CH_3OH (0.5 M)	117	(-)	92	2021	[54]
Ni foam	KOH 1 M	500	3.94	90	2020	[52]
Ni foam	KOH 1 M	405	2.74	89	2020	[57]
Ni foam	KOH 2 M	100	65.40	80	2020	[53]
Ni gauze	KOH 5 M	1000	(-)	80	2019	[64]
Ni foam	KOH 10 M	450	(-)	50	2018	[62]

was saturated with Ar, under a flow rate of 100 mL·min^{-1}, to remove any dissolved oxygen. Immediately after dipping the GCE into the electrolyte, and employing the feed stream of 100 mL·min^{-1}, the potential was maintained at 0.4 V for 30 min to avoid exposure to open circuit potential. While ensuring inert gas blanketing, the catalyst was activated through 100 cyclic voltammograms (CV) between 0 and 1.8 V at 100 mV·s^{-1}, without rotation. Subsequently, for each catalyst 3 CVs were retrieved between 0 and 1.8 V with a scan rate of 20 mV·s^{-1}. To obtain the OER-mass activity, linear sweep voltammetry (LSV) was carried out between 1.2 and 1.8 V (vs. RHE) at 20 mV·s^{-1} at 1600 RPM. Additionally, electrochemical impedance spectroscopy (EIS) was also performed to measure the ohmic resistance of the electrolyte in potentiostatic mode (0.4 V vs. RHE) using 5 mV of amplitude between 1 kHz and 0.1 Hz.

2.2. CO_2 flow electrolyzer experimental setup

All the experiments concerning the continuous electrocatalytic reduction of CO_2 to formate reported throughout this manuscript were developed in a filter press reactor, using the experimental laboratory system whose general diagram is shown in Fig. 1.

The experiments to test Ni-based materials as a catalyst in the counter electrode were carried out using a liquid feed at the cathode side of the filter-press reactor, which is a configuration that we have widely studied previously and that allows a reliable comparison with previous approaches [68]. Electrochemical experiments were carried out at least in duplicate with an operating time of 60 min under ambient conditions of temperature and pressure. Two magnetically stirred glass tanks served as the reservoirs for the catholyte and the anolyte. On the one hand, an aqueous solution of 0.45 M $KHCO_3$ + 0.5 M KCl was used as a catholyte, while a solution of KOH was used as an anolyte. Each electrolyte was circulated through its own compartment, with only one pass through the reactor, using peristaltic pumps (Watson Marlow 320, Watson Marlow Pumps Group) with a flow rate of (i) 0.7, 1.5 or 5.7 mL·min^{-1} (catholyte stream) and (ii) 5.7, 11.4, 17.1 or 22.8 mL·min^{-1} (anolyte stream), and an anolyte concentration of 0.5, 0.75, 1, 1.5 or 2 M that varied depending on the experiment. A pure CO_2 stream was fed to the cathodic compartment with a flow rate of 0.2 L·min^{-1}. Besides, experiments were carried out at galvanostatic conditions with a potentiostat-galvanostat (Arbin Instruments, MSTAT4) using a current density of 45, 90, 150, or 200 mA·cm^{-2}.

As depicted in Fig. 1, the main element of the experimental setup is the electrochemical reactor (Micro Flow Cell, ElectroCell A/S). Fig. 2 shows a schematic representation of the filter press reactor configuration, which consists of two-compartments divided by a Nafion™ 117 cationic-exchange membrane. The working electrode was a Bi Gas Diffusion Electrode (Bi-GDE), while a Ni particulate electrode (Ni-PE) was employed as a counter electrode, as detailed in the following subsections. Both electrodes had an active area of 10 cm^2. A leak-free Ag/AgCl 3.4 M KCl reference electrode was placed in a PTFE frame at the cathodic compartment of the filter press reactor.

The samples were taken at the outlet stream of the cathode side of the electrochemical reactor at different times of operation (15, 30, 45, and 60 min) and the average value of the formate concentration was obtained for each experiment. This concentration was analyzed by ion chromatography (Dionex ICS 1100) equipped with an AS9-HC column.

2.3. Counter electrodes manufacturing

For the electrocatalytic reduction of CO_2 to formate, a Ni-PE was used as the counter electrode. As illustrated in Fig. 3a, the Ni-PE configuration is composed of two layers: (i) a hydrophilic carbon paper carbonaceous support, and (ii) a catalytic layer.

Toray Carbon Paper TGH-60 was used as carbonaceous support for the fabrication of the counter electrodes. Then the following element is the catalyst layer, which was deposited using a manual air-brushing technique. This layer was deposited through an ink which was prepared with the catalyst and the binder in a proportion of 70–30 wt %, diluted in isopropanol (99.5 % Extradry, AcroSeal) to obtain a final suspension of 3 wt % in solids. Before spraying, the ink, was introduced in an ultrasonic bath (Selecta ultrasonic bath operating at 50/60 kHz, 360 power output) for 30 min for a complete mixture and homogenization. Consequently, the ink was sprayed in an area of 10 cm^2 with constant heating until it reached loadings of (i) 0.75 mg·cm^{-2}, (ii) 1.5 mg·cm^{-2}, (iii) 2.25 mg·cm^{-2}, or (iv) 3 mg·cm^{-2} of NiO. The catalysts selected for the preparation of anodes were the 2-NiO catalysts since gave the best results in the electrochemical characterization explained in Section 3.1. Moreover, the binders employed in this study were: (i) Nafion™ (Nafion™ D-521, 5 % (w/w) in water/1-propanol, dispersion ≥ 0.92 meq/g exchange, VWR), or (ii) Sustainion® (Sustainion® XA-9 Alkaline Ionomer 5 % in ethanol, Dioxide Materials).

2.4. Counter electrodes characterisation

Scanning electron microscopy with energy dispersive spectroscopy (SEM-EDS, PhenomPro XL Desktop SEM) was employed to analyze the surface and cross-section morphology of the counter electrodes, and to assess the element distribution at their surface. SEM images were obtained at several magnifications 320 x and 1850 x using backscattered electrons mode. Raman spectroscopy was also performed in an inVia

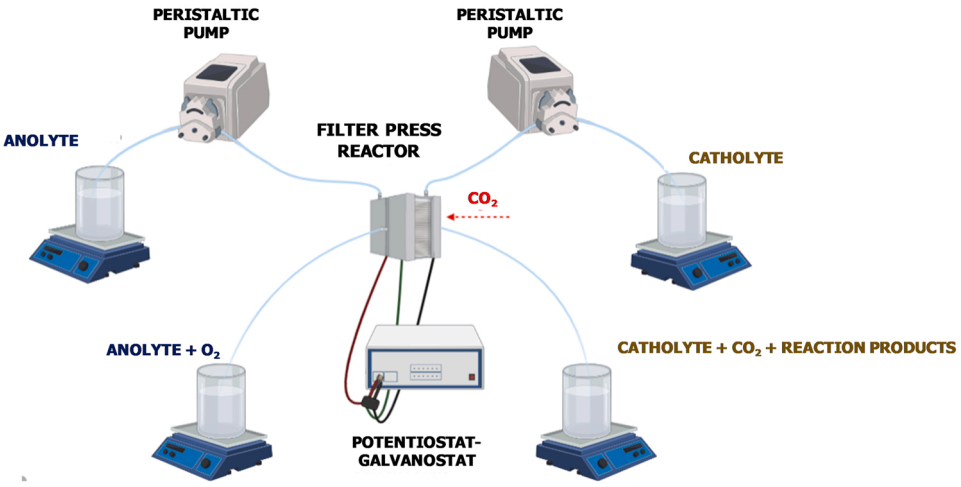

Fig. 1. Experimental setup used for the continuous electrocatalytic reduction of CO_2 to formate in a filter press reactor.

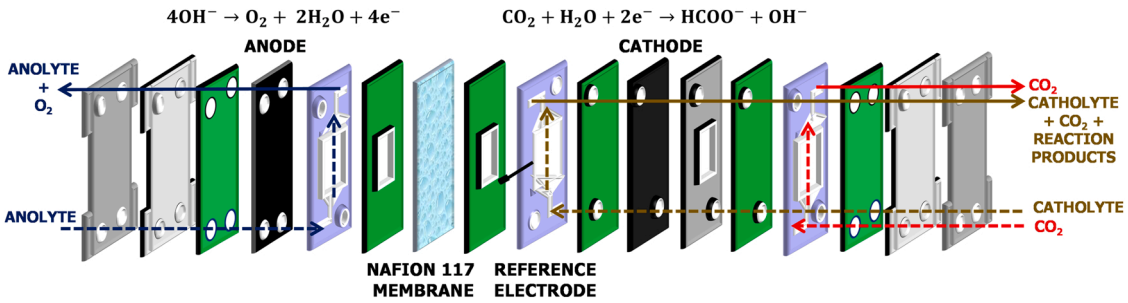

Fig. 2. Filter press reactor configuration used for the continuous electrocatalytic reduction of CO_2 to formate in a filter press reactor.

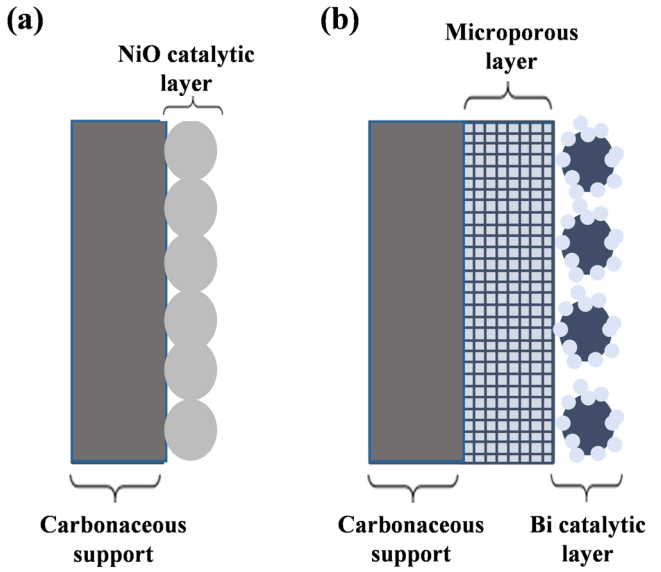

Fig. 3. Composition of (a) the anodic particulate electrode composed of: (i) Carbonaceous support, and (ii) NiO catalytic layer, and (b) the cathode side GDE composed of: (i) Carbonaceous support, (ii) microporous layer, and (iii) Bi catalytic layer.

confocal Raman microscope equipped with 532 nm laser excitation (100 × and an exposure of 5 s).

2.5. Working electrodes manufacturing

A Bi-GDE was used as the working electrode to carry out the CO_2 electroreduction to formate. Regarding the configuration of the GDE, it is composed of three layers: (i) a carbonaceous support, (ii) a microporous layer, and (iii) a catalytic layer, as depicted in Fig. 3b.

The carbonaceous support was the same as described previously in the fabrication of anodes. The microporous layer, which was also deposited using an air-brushing technique, was composed of Vulcan XC-72R, PTFE (Polytetrafluoroethylene preparation, 60 wt % dispersion in H_2O, Sigma-Aldrich) in a proportion of 40–60 wt %, diluted in to obtain a similar suspension than previously reported. Consequently, this layer was sintered at 623 K in a muffle furnace (PR series, Hobersal) for a period of time of 30 min. The catalytic ink was composed of Bi carbon-supported nanoparticles, which act as an electrocatalyst, Nafion™, and isopropanol. The proportion of these components was the same as reported before for the fabrication of this layer in anodes. This ink was also sonicated for 30 min approximately, and it was sprayed until reaching a Bi loading of 0.75 mg·cm^{-2}, which is considered the optimal loading. On the one hand, the Bi carbon-supported nanoparticles were synthesized and characterized, using $BiCl_3$ as a precursor and Vulcan XC-72R as the carbon support [24]. On the other hand, the Bi/C-GDE has been characterized in previous works of the research group [34,68].

2.6. Figures of merit

Firstly, to assess the oxygen evolution reaction (OER) of the Ni-based materials tested in the RDE (described in Section 2.1), the mass activity, the geometric activity, and Tafel slopes were used as figures of merit. These three parameters are commonly used in the literature to evaluate and compare different materials. The mass activity represents the current per unit of mass of catalyst (mA·mg^{-1}), while the geometric activity defines the current per unit geometric area of glassy carbon electrode (mA·cm^{-2}) [69]. Moreover, Tafel slopes (mV·dec^{-1}) correlate the current density applied with the overpotential [70]. To compare the OER activity of the different Ni-based catalysts, the kinetic activities were compared at 1.55 V vs RHE. This potential was chosen since it was low enough to avoid the mass transport governed by polarisation [71].

The performance of the electrochemical conversion of CO_2 to formate is assessed by the concentration of product (g·L^{-1}), the Faradaic efficiency for formate (%), the rate (mmol·m^{-2}·s^{-1}), and the consumption of energy of formate (kWh·kmol^{-1}). The different equations employed to analyze these key performance criteria can be found in Section 1 of the Supplementary Information.

2.7. Experimental conditions of previous approaches using DSA/O2

The performance of the CO_2 electroreduction to formate process using Ni-based particulate electrodes is compared with respect to the results employing a DSA/O_2 as an anode using the same filter press reactor configuration and the same operating conditions (i.e. CO_2 flow, catholyte flow per geometric surface area, Bi catalyst loading and current density) [68]. Although the anolyte concentration and anolyte flow per geometric surface area were 1 M and 0.57 mL·min^{-1}·cm^{-2}, respectively, with a commercial dimensionally stable anode [DSA/O_2 (Ir-MMO (mixed metal oxide) on platinum), Electrocell], composed by both Ti and Ir oxides, these variables and the NiO catalyst loading have been studied in detail in the following subsections.

3. Results and discussion

3.1. Electrochemical measurements of Ni-based materials

Fig. 4 shows the CVs obtained with the different NiO catalysts using a scan rate of 20 mV·s^{-1}. The first results showed a higher OER activity for 2-NiO catalysts with respect to the use of 1-NiO catalysts. Besides, both catalysts present a cathodic contribution, which is attributed to the reduction of NiO to Ni, at ca. 1.35 V. After this first analysis, it can be concluded that 2-NiO catalysts have much more favorable OER activity than the 1-NiO catalyst.

On the other side, the results obtained from the LSV analysis are represented in Fig. 5 for both 1-NiO and 2-NiO catalysts. These results are shown in terms of the current per working electrode geometric area (Fig. 5a) and the current per mass of the active metal (Fig. 5b). For both analyses, it is important to remark that the electrolyte resistances, whose values were obtained through EIS (see Supplementary Information,

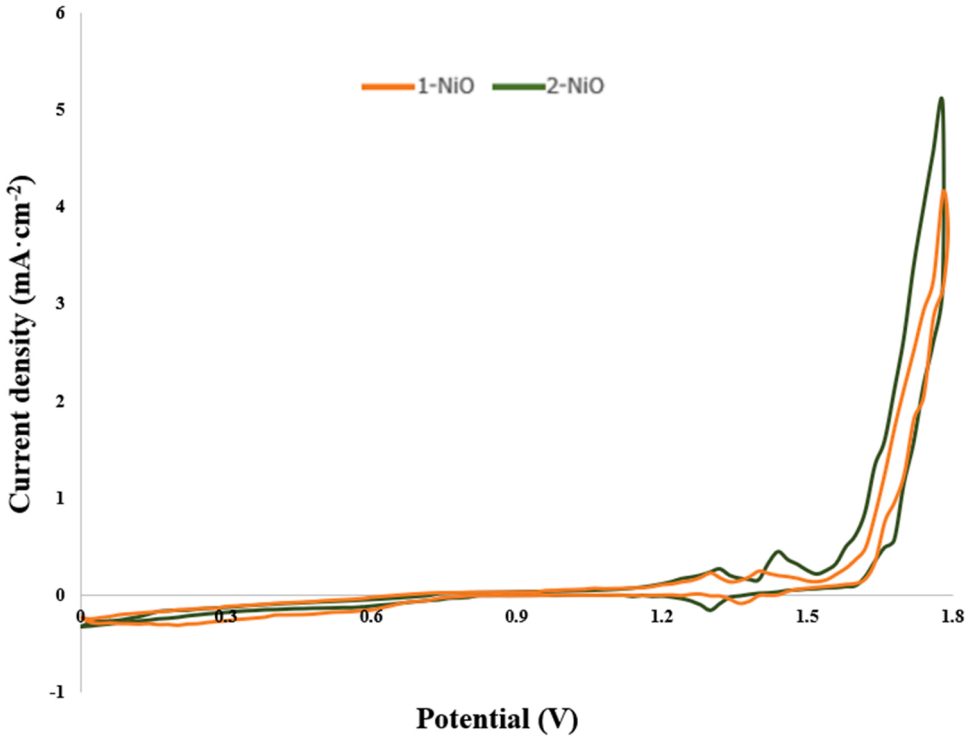

Fig. 4. CVs after 3 cycles in 1 M $KOH_{(aq)}$ under a purged electrolyte (scan rate of 20 $mV \cdot s^{-1}$) using the Ni-based materials: (A) 1-NiO and (B) 2-NiO.

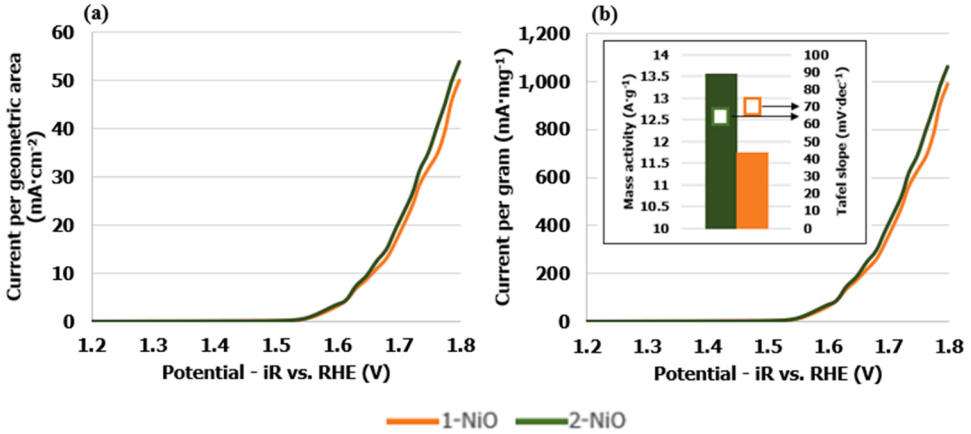

Fig. 5. Linear sweep voltammetry (LSV) curves for OER at a scan rate of 20 $mV \cdot s^{-1}$ conducted in a purged 1 M $KOH_{(aq)}$ electrolyte, in terms of (a) the current per electrode geometric area and (b) current per gram of the active metal. In the inset, the mass activity at 1.55 V vs. RHE and the Tafel slope is compared.

Section 2) have been removed. The LSV analysis confirmed the results obtained previously in CVs. As illustrated in Fig. 5a, the OER activity of 2-NiO catalyst is higher with respect to the use of 1-NiO catalyst, achieving higher values of current per area at 1.8 V. Besides, the 2-NiO catalyst had the highest mass activity (13.55 $A \cdot g^{-1}$) at 1.55 V vs. RHE, which corresponds to a geometric activity value of 0.69 $mA \cdot cm^{-2}$, as well as the lowest Tafel slope (61.6 $mV \cdot dec^{-1}$). This value of potential is used to compare the OER activities of both catalysts with other Ni-based catalysts reported in the literature [71], as summarized in Table 2.

Thus, the catalysts evaluated in this work have a higher mass activity than other Ni-based catalysts used in the literature to carry out the OER, and therefore, higher geometric activity values, whose values are also indicated in Table 2. On the other hand, the 2-NiO catalyst has a Tafel Slope of 61.6 $mV \cdot dec^{-1}$, lower than other Tafel slopes reported for other Ni catalysts. This implies that the catalysts tested in this section have the most favorable OER kinetic performance of all the materials compared (Table 2). Thus, the 2-NiO catalyst was chosen as the anodic electrocatalyst for subsequent tests of the reduction of CO_2 to $HCOO^-$ in a continuous way in a filter press reactor.

3.2. Electrodes characterization

From the results obtained in the previous Section (3.1), the 2-NiO catalyst was chosen to prepare the Ni-PEs. These electrodes were also characterized (surface and cross-section) by SEM/EDX. Fig. 6 reports some representative SEM images obtained using backscattered electrons of catalysts layers composed of 2-NiO catalysts sprayed using both Nafion™ and Sustainion® as ionomer and a loading of 1.5 mg $NiO \cdot cm^{-2}$. As illustrated in Figs. 6a and 6e, the sprayed catalyst layer appears to be homogeneous and the fibers are completely covered with ionomer and although some fractures are clearly visible, at much higher magnification (Figs. 6b and 6d), it is possible to visualize the good

Table 2
Mass activity, geometric activity and Tafel slope values of NiO catalysts analyzed in this section, as well as other Ni-based catalysts reported in the literature for a potential value of 1.55 V vs. RHE.

Catalysts ($mA{\cdot}cm^{-2}$)	Mass activity ($A{\cdot}g^{-1}$)	Geometric activity ($mA{\cdot}cm^{-2}$)	Tafel slope ($mV{\cdot}dec^{-1}$)	Reference
2-NiO	13.55	0.69	61.6	This work
1-NiO	11.74	0.60	74.1	This work
Ni (Alfa Aesar)	0.1	$1.4{\cdot}10^{-3}$	93	69
Ni (PlasmaChem GmbH)	6.5	$5.7{\cdot}10^{-2}$	101	
NiO (Alfa Aesar)	$8{\cdot}10^{-4}$	$3{\cdot}10^{-6}$	149	
$Fe_{55}Ni_{28}Co_{17}$ (US Research Nanomaterials Inc.)	0.1	$5{\cdot}10^{-4}$	99	
$NiFe_2O_4$ (US Research Nanomaterials Inc.)	1.8	$4.8{\cdot}10^{-3}$	86	

dispersion of the NiO catalysts. Besides having dispersed the same concentration of Sustainion® and Nafion™, the catalyst layer comprising Sustainion® as binder appears to have generated a slightly more cohesive microstructure with enhanced dispersion of catalyst nanoparticles (Fig. 6d), which may infer for greater stability of the electrode throughout long term experiments. From the analysis of the cross-section (Fig. 6c), the thickness of the NiO catalytic loading is estimated to be about 200 μm approximately, when using a loading of 1.5 $mg{\cdot}cm^{-2}$. Besides, both surface and cross-section of Ni-PEs for NiO catalyst loading of 0.75 $mg{\cdot}cm^{-2}$ (Fig. S2), 2.25 $mg{\cdot}cm^{-2}$ (Figs. S3), and 3 $mg{\cdot}cm^{-2}$ (Fig. S4) are included in Section 2 of the Supplementary Information.

Raman spectroscopy was also carried out to study the degree of crystallization of carbon. The D band at 1340 cm^{-1} is ascribed to the disorder-induced mode, while a relatively sharp G band at 1575 cm^{-1} is ascribed to the E2g mode from the sp^2 carbon [72]. The relative ratios of D bands to G bands (ID/IG) in Raman spectra, indicates the crystallization degree of graphitic carbon. The ratio of intensity of D/G bands is a measure of the defects present on graphene structure. The G band is a result of in-plane vibrations of sp^2bonded carbon atoms whereas the D band is due to out of plane vibrations attributed to the presence of structural defects. The D/G ratio of carbon structures is commonly compared to those measured for graphene oxide and reduced graphene oxide (ID/IG=1), indicating that high quality 3D graphite carbon was formed [72]. Likewise, there was a 2D band at 2676 cm^{-1}.

From Table 3 is becomes evident the highly crystalline structure for the carbon particles after the electrochemical measurements. This is important to ensure high electrical conductivity and hints for very low corrosion. Nonetheless, the electrode with the 1.5 $mg{\cdot}cm^{-2}$ yields the most crystalline among the electrodes containing Nafion™ ionomer. This suggests that few defects or capacitive groups were generated on the carbon particles, which is very important to maintain the electrode porosity and low mass transport overpotentials at high current densities [73].

3.3. *Preliminary assessment of Ni-based particulate electrodes*

Preliminary tests were carried out for assessing the feasibility of Ni-based particulate electrodes by studying their performance at different values of current density (i.e. 45, 90, 150, and 200 $mA{\cdot}cm^{-2}$), and with different catholyte flows per geometric surface area (i.e. 0.57, 0.15, and 0.07 $mL{\cdot}min^{-1}{\cdot}cm^{-2}$). In these experiments, both anolyte concentration and anolyte flow per geometric surface area were 1 M and 0.57 $mL{\cdot}min^{-1}{\cdot}cm^{-2}$, respectively, similar to previous recent studies [68]. In addition, the 2-NiO catalyst loading was 0.75 $mg{\cdot}cm^{-2}$. Table 4 summarizes the main results achieved in terms of formate concentration, Faradaic Efficiency, rate, and energy consumption.

Operating with the same catholyte flow per geometric surface area, a

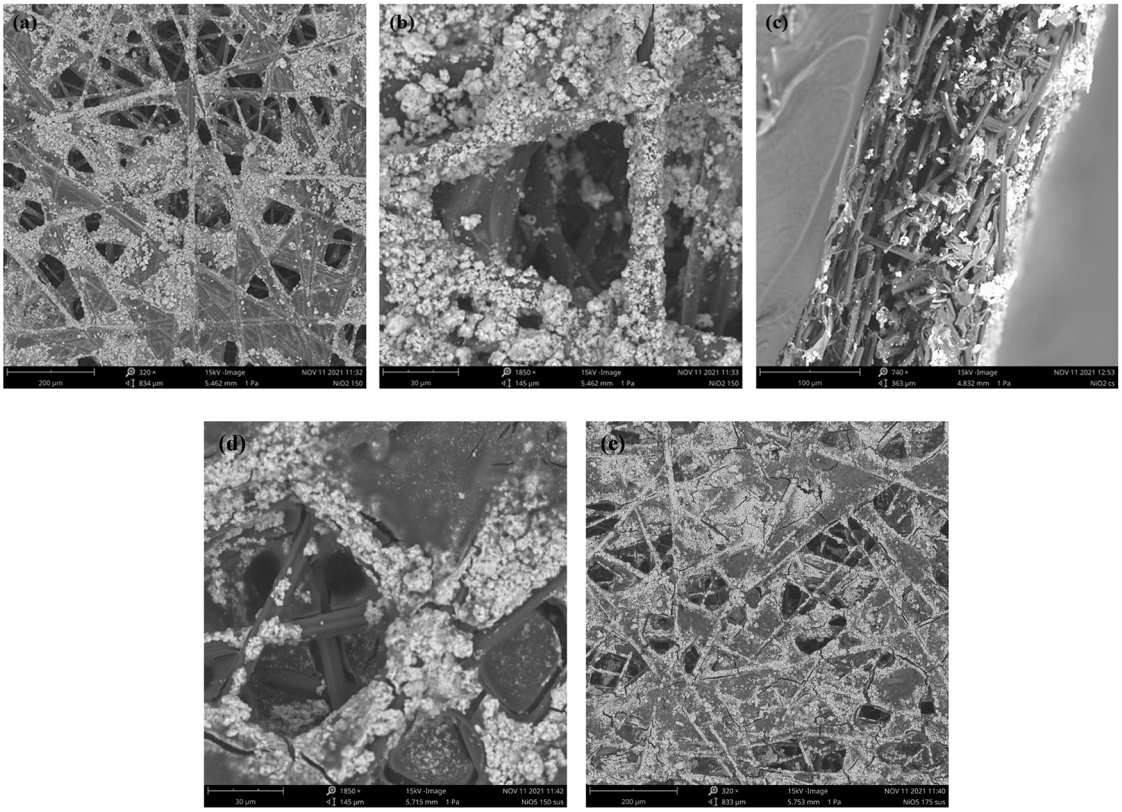

Fig. 6. SEM images of the (i) Nafion™ Ni-PEs for NiO catalyst loading of 1.5 $mg{\cdot}cm^{-2}$, (a, b) surface at 320 x and 1850 x magnification, respectively and (c) cross section, and (ii) Sustainion® Ni-PEs for 2-NiO catalyst loading of 1.5 $mg{\cdot}cm^{-2}$, (d, e) surface at 1850 x and 320 X magnification.

Table 3
Raman spectroscopy of electrodes with different Ni loading (D/G ratio).

Ni loading	0.75 mg·cm^{-2} Nafion™	1 mg·cm^{-2} Nafion™	1.5 mg·cm^{-2} Nafion™	1.5 mg·cm^{-2} Sustainion®	2 mg·cm^{-2} Nafion™
D/G	0.46	0.57	0.60	0.48	0.58

Table 4
Results using Bi/C-GDE and Ni-PE as cathode and anode, respectively, in a continuous CO_2 electroreduction to formate process in the range of current density from 45 to 200 mA·cm^{-2}, and catholyte flow per geometric surface area from 0.07 to 0.57 mL·min^{-1}·cm^{-2} at a Bi catalyst loading = 0.75 mg·cm^{-2}, a NiO catalyst loading = 0.75 mg·cm^{-2}, an anolyte concentration = 1 M, and an anolyte flow per geometric surface area = 0.57 mL·min^{-1}·cm^{-2}.

Current density, (mA·cm^{-2})	Catholyte flow per geometric surface area, (mL·min^{-1}·cm^{-2})	Formate concentration, (g·L^{-1})	Faradaic Efficiency for formate, (%)	Formate rate, (mmol·m^{-2}·s^{-1})	Energy consumption, (kWh·kmol^{-1})	Standard deviation, (%)	Cathode potential, (V)	Absolute cell potential, (V)
45	0.57	0.67	61.14	1.43	299	0.65	-0.67	3.42
90		1.70	77.20	3.60	329	2.70	-1.54	4.79
150		2.05	55.67	4.32	522	22.00	-1.88	5.30
200		2.40	48.95	5.07	711	20.00	-2.02	6.35
45	0.15	2.80	66.77	1.55	265	2.34	-0.60	3.31
90		5.50	65.24	3.04	335	4.88	-1.27	4.08
150		11.27	82.40	6.40	339	11.85	-1.67	5.20
200		13.42	71.47	7.15	440	9.38	-1.83	5.85
45	0.07	4.71	52.40	1.23	337	1.17	-0.69	3.30
90		9.30	51.73	2.41	441	10.16	-1.20	4.23
150		13.73	45.80	3.56	595	3.80	-1.73	5.09

raise in the current density represents an increase in the formate concentration at the outlet stream of the electrochemical reactor, as well as in the formate rate and in the energy consumption. In this sense, when the current density increases from 45 to 200 mA·cm^{-2} with a catholyte flow per geometric surface area of 0.15 mL·min^{-1}·cm^{-2}, the formate concentration obtained is increased approximately 400 % (from 2.80 to 13.42 g·L^{-1}). In addition, increasing the current density from 45 to 200 mA·cm^{-2} allows observing the same trend in the formate rate and in the energy consumption operating with a catholyte flow rate per geometric surface area of 0.57 mL·min^{-1}·cm^{-2}. In this case, the formate rate increases in 254 points in percentage (from 1.43 to 5.10 mmol·m^{-2}·s^{-1}), while the energy consumption rises in 137 % (from 299 to 711 kWh·kmol^{-1}). On the other hand, the results confirm, as expected, that the Faradaic Efficiency towards formate decreases when the current density increases.

Regarding the study of the influence of the catholyte flow per geometric surface area, this variable is of special interest since it allows achieving a more concentrated product in the output stream at the cathode side of the electrochemical reactor. In general, the results summarized in Table 4 show that the formate concentration increases as the catholyte flow per geometric surface area decreases. In this way, lowering the catholyte flow from 0.57 to 0.07 mL·min^{-1}·cm^{-2} with a current density of 90 mA·cm^{-2} causes an increase in the concentration from 1.70 to 9.30 g·L^{-1} of formate. Similarly, rising the current density from 90 to 150 mA·cm^{-2} and employing the same catholyte flow range, the concentration suffers an increase of up to 570 %, highlighting the concentrations achieved at 0.07 mL·min^{-1}·cm^{-2}, up to 13.73 g·L^{-1}, similar to those obtained under operation conditions of 200 mA·cm^{-2} and 0.15 mL·min^{-1}·cm^{-2} (13.42 g·L^{-1}).

The results obtained by employing Ni-PE as counter electrodes to carry out the OER in the anodic compartment of the filter-press electrochemical reactor, summarized in Table 4, could be considered as promising. In general, comparing these results with those achieved in previous studies with a DSA/O_2 [68] under the same operating conditions, the figures of merit are close to, and even better than, those obtained previously. The detailed comparisons at the different tests are reported in Table S1 of the Supplementary Information. Thus, these preliminary but promising results with Ni-PE encouraged us to carry out further studies, taking into account the possibility of assessing the influence of other key variables in the electrochemical process, and particularly related to the anodic compartment of the filter-press cell, such as the NiO catalyst loading, the anolyte concentration, and the anolyte flow per geometric surface area, for further improvement of process performance.

3.4. Influence of key variables in the anodic compartment

Following the promising results reported in the previous section with Ni-PE anodes, this section will present the further in-depth studies that were subsequently performed for studying the influence of NiO catalyst loading, the anolyte concentration, and the anolyte flow per geometric surface area.

In this sense, a first study was carried out to analyze the influence of NiO catalyst loading in the CO_2 electroreduction to formate process with respect to that obtained with a DSA/O_2. In the initial tests (Section 3.3), the NiO loading was 0.75 mg·cm^{-2}, but the results showed that, when compared with similar experiments with DSA/O_2, a higher cell potential was measured in the electrochemical reactor, and in particular in the anodic compartment (Table S1 of the Supplementary Information). This could initially be directly attributed to a lack of active sites on the anode surface as a consequence of insufficient NiO catalyst loading. Therefore, additional tests were developed at NiO catalyst loading of 1.5, 2.25, and 3 mg·cm^{-2}. In order to make a rigorous comparison with the previous subsection, the experiments were carried out at a current density of 90 mA·cm^{-2} and a catholyte flow rate per geometric surface area of 0.15 mL·min^{-1}·cm^{-2}. Fig. 7 depicts the results achieved in terms of formate concentration, energy consumption, and potential in the anodic compartment at different NiO catalyst loadings.

As can be seen in Fig. 7 (specific values for all the experiments of the manuscript are reported in Table S2 of the Supplementary Information), rising the NiO catalyst loading on the anode surface from 0.75 to 3 mg·cm^{-2} reduces the potential in the anodic compartment by approximately 23 %. In contrast, the formate concentration increases up to 30 % (from 5.5 to 7.1 g·L^{-1} of formate) when the NiO catalyst loading raises from 0.75 to 1.5 mg·cm^{-2}. In addition, when the loading is increased from 1.5 to 3 mg·cm^{-2}, the formate concentration falls back slightly to a value of 6.4 g·L^{-1} of formate. As a consequence of a reduction in the anodic potential and an increase in the formate concentration in the range of NiO catalyst loading from 0.75 to 1.5 mg·cm^{-2}, the energy consumption per kmol of formate was reduced

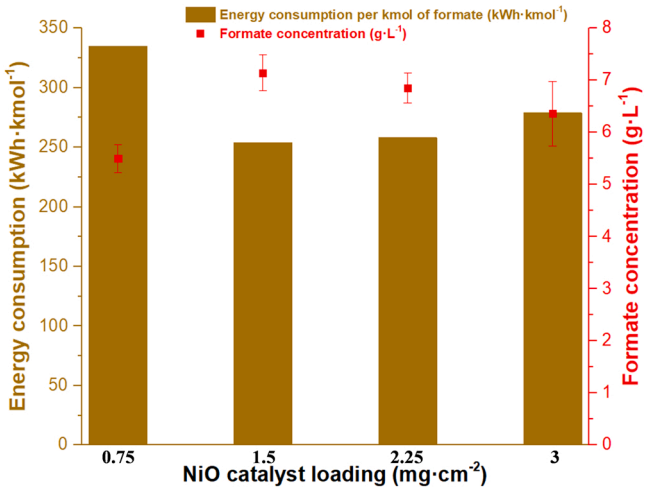

Fig. 7. Results using Bi/C-GDE and Ni-PE as cathode and anode, respectively, in a continuous CO_2 electroreduction to formate process for NiO catalyst loadings of 0.75, 1.5, 2.25 and 3 mg·cm^{-2} at a current density = 90 mA·cm^{-2}, a catholyte flow per geometric surface area = 0.15 mL·min^{-1}·cm^{-2}, a Bi catalyst loading = 0.75 mg·cm^{-2}, an anolyte concentration = 1 M, and an anolyte flow per geometric surface area = 0.57 mL·min^{-1}·cm^{-2}.

by approximately 24 % (from 335 to 254 kWh·kmol^{-1}). These results confirm the hypothesis of the great influence of the NiO catalyst loading on the process performance and, consequently, suggests that more efforts are necessary to evaluate the influence of the anolyte concentration and flow per geometric surface area.

Thus, after obtaining an optimal value of NiO catalyst loading of 1.5 mg·cm^{-2} for the continuous electrocatalytic reduction of CO_2 to formate, the influence of both anolyte concentration (Table S3 of the Supplementary Information) and anolyte flow per geometric surface area (Table S4) was studied. Both variables play an important role in the oxygen evolution reaction that takes place in the anode, which supplies the electrons for the CO_2 electroreduction.

Firstly, the values of anolyte concentration studied were 0.5, 0.75, 1, 1.5, and 2 M which were chosen since they are the most common electrolyte concentrations employed in the literature. Fig. 8a represents the variation of formate concentration and the influence on the formate production rate in operation under different anolyte concentration. Fig. 8b shows the influence of anolyte concentration on Faradaic Efficiency for formate vs. the energy consumption needed to produce formate. In this way, a threshold was obtained for an anolyte concentration of 1 M, achieving a maximum formate concentration of 7.14 g·L^{-1}. The formate outlet concentration was lower when the circulated anolyte concentration differed from 1 M KOH, e.g. when the concentration is reduced to 0.75 M, the concentration of formate is decreased to 6.80 g·L^{-1}, and if the anolyte concentration lowers even more to 0.5 M, the concentration reaches values of only 5.85 g·L^{-1} of produced formate. The same phenomenon was observed when the anolyte concentration was increased to values of 1.5, and 2 M, reaching values of formate concentration of 6.52 and 5.84 g·L^{-1}, respectively, showing a reduction of 18.2 % with respect to an anolyte concentration of 1 M. Regarding the formate rate (Fig. 8b), the optimum value was also attained for an anolyte concentration of 1 M, achieving a value of approximately 4 mmol·m^{-2}·s^{-1}.

The variation of the Faradaic Efficiency for formate with the anolyte concentration is also represented in Fig. 8b, showing the same trend as the formate concentration and rate. The highest Faradaic Efficiency for formate (85 %) was achieved with an anolyte concentration of 1 M, while using KOH concentrations of 0.5 or 2 M this efficiency lowers to values of approximately 70 %. These results could be attributed to the fact that the pH of the anolyte stream plays a key role in the oxygen evolution reaction, while increasing this concentration up to 2 M

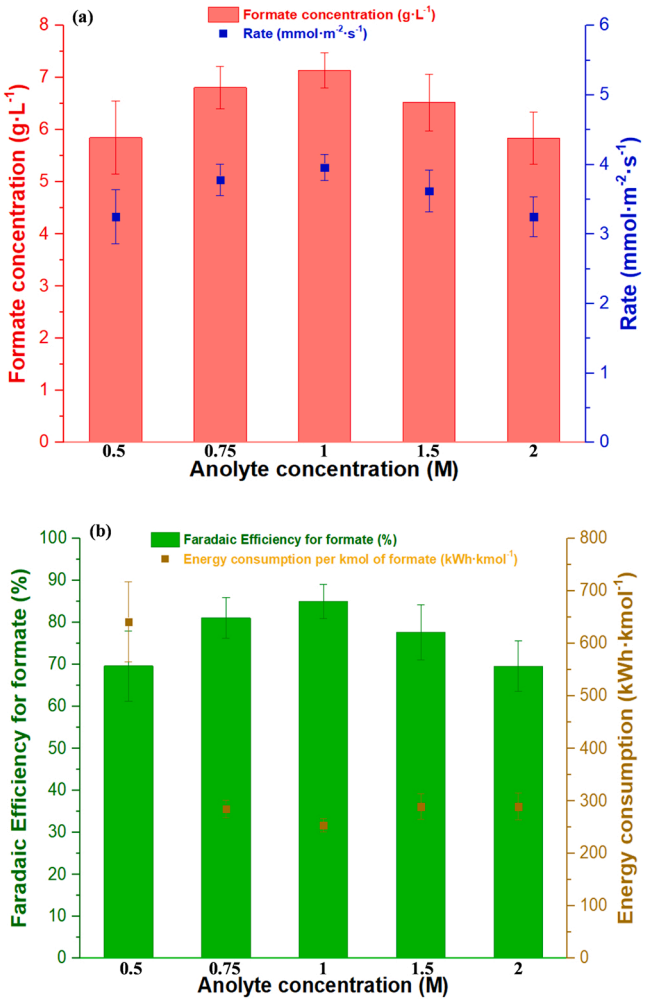

Fig. 8. Influence of anolyte concentration on (a) formate concentration (g·L^{-1}) and rate (mmol·m^{-2}·s^{-1}) and (b) the Faradaic Efficiency for formate (%) and energy consumption per kmol of formate (kWh·kmol^{-1}) in the anolyte concentration range of 0.5 – 2 M, at a current density = 90 mA·cm^{-2}, a catholyte flow per geometric surface area = 0.15 mL·min^{-1}·cm^{-2}, a NiO catalyst loading = 1.5 mg·cm^{-2}, a Bi catalyst loading = 0.75 mg·cm^{-2}, and an anolyte flow per geometric surface area = 0.57 mL·min^{-1}·cm^{-2}.

probably causes a degradation of the anodes.

The energy consumption was also affected by the anolyte concentration, being mainly influenced by the resistance of the cell during each experiment. In this sense, despite the fact, promising values of energy consumptions were obtained for concentrations of 0.75, 1.5, and 2 M, the lowest value of this figure is observed for anolyte concentrations of 1 M, reaching values of only 254 kWh·kmol^{-1}. Besides, the energy consumption was increased by 152 % (641 kWh·kmol^{-1}) by employing a KOH concentration of 0.5 M due to a reduction in the anodic compartment conductivity.

Finally, the influence of the anolyte flow per geometric surface area was assessed, for different values ranging from 0.57 to 2.28 mL·min^{-1}·cm^{-2}. Besides, more tests were carried out at lower values than 0.57 mL·min^{-1}·cm^{-2} of anolyte flow per geometric surface area, but the absolute cell potentials were considerably increased, so these flow conditions were dismissed. As can be checked in Fig. 9a, the best results were achieved operating with an anolyte flow per geometric surface area of 1.14 mL·min^{-1}·cm^{-2}, obtaining a formate concentration up to 8.65 g·L^{-1}, and a rate of 4.80 mmol·m^{-2}·s^{-1}. On the other hand, Fig. 9b depicts the results in terms of Faradaic Efficiency for formate. In this sense, it is important to highlight that Faradaic Efficiencies close to

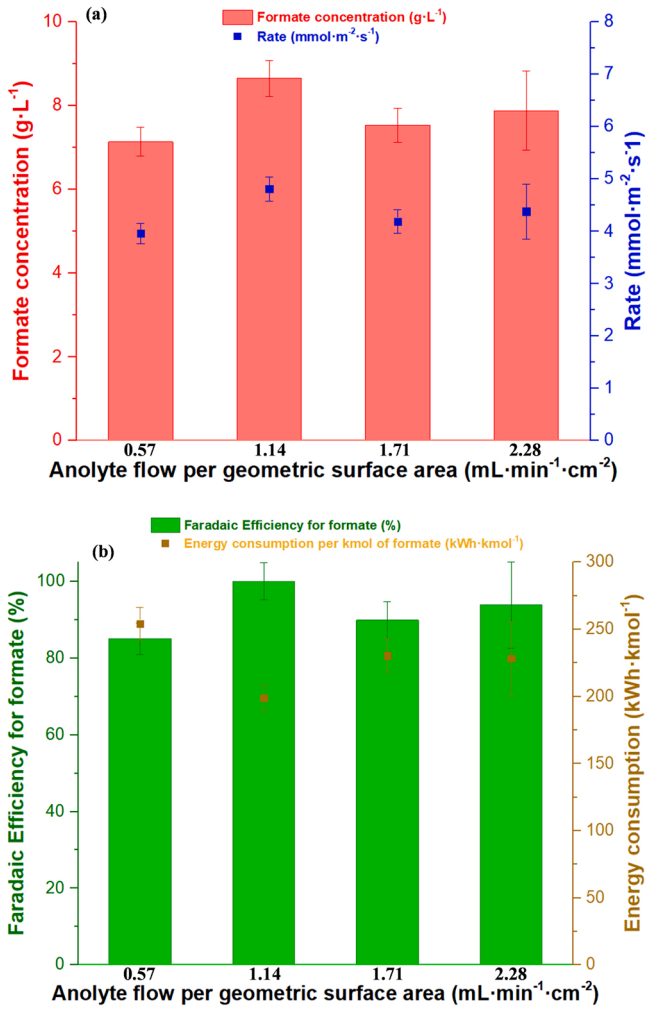

Fig. 9. Influence of anolyte flow per geometric surface area on (a) formate concentration ($g{\cdot}L^{-1}$) and rate ($mmol{\cdot}m^{-2}{\cdot}s^{-1}$) and (b) the Faradaic Efficiency for formate (%) and energy consumption per kmol of formate ($kWh{\cdot}kmol^{-1}$) in the anolyte flow per geometric surface area range of 0.57 – 2.28 $mL{\cdot}min^{-1}{\cdot}cm^{-2}$, at a current density = 90 $mA{\cdot}cm^{-2}$, a catholyte flow per geometric surface area = 0.15 $mL{\cdot}min^{-1}{\cdot}cm^{-2}$, a NiO catalyst loading = 1.5 $mg{\cdot}cm^{-2}$, a Bi catalyst loading = 0.75 $mg{\cdot}cm^{-2}$, and an anolyte concentration = 1 M.

100 % were achieved working with an anolyte flow per geometric surface area of 1.14 $mL{\cdot}min^{-1}{\cdot}cm^{-2}$. Similarly, the lowest energy consumption per kmol of formate was reached at the same anolyte flow, achieving consumptions of only 200 $kWh{\cdot}kmol^{-1}$, 22 points in percentage lower than the energy consumption observed with an anolyte flow per geometric surface area of 0.57 $mL{\cdot}min^{-1}{\cdot}cm^{-2}$.

In general, after analyzing the influence of NiO catalyst loading, the anolyte concentration, and the anolyte flow per geometric surface area, the results in terms of all the figures of merit were enhanced with respect to the preliminary tests developed in the previous subsection. The formate concentration and the rate were increased from 5.5 to 8.65 $g{\cdot}L^{-1}$ of formate, and from 3.04 to 4.80 $mmol{\cdot}m^{-2}{\cdot}s^{-1}$, respectively. It is important to note that after analyzing the influence of these variables, the Faradaic Efficiency for formate reaches values of 100 % and energy consumptions of only 198 $kWh{\cdot}kmol^{-1}$. Despite the fact that competitive results were achieved in terms of all the figures of merit, further research is required to enhance the durability of the counter electrode, which is desirable for future implementation of the process at the industrial scale.

3.5. Further improvements in the counter electrode

The optimization of the binder ratio/type used to prepare the particulate electrodes appears as clear possibilities for further tuning the Ni-PE performance. According to some recent studies published in the field of CO_2 electroreduction [74,75] and water electrolysis in alkaline medium [76], the use of different types of ionomers, particularly Sustainion® (based of imidazolium functionalized styrene) as an anion exchange ionomer, plays an essential role for enhancing the electrochemical process due to its high ion exchange capacity in alkaline media (ca.0.9–1.2 $mmequiv.g^{-1}$). The use of Sustainion® as binder at the catalyst layer level typically increases the local pH which directly influences the reaction mechanism of the OER [77]. For this purpose, Sustainion® anodes were also prepared and their performance was assessed while applying the best operating conditions achieved in the last sections to make a rigorous comparison with anodes using Nafion™ as binder. In detail, a NiO catalyst with loading of 1.5 $mg{\cdot}cm^{-2}$ was used to prepare de anode, an anolyte concentration of 1 M KOH was applied under an anolyte flow rate of 11.4 $mL{\cdot}min^{-1}$ and a catholyte flow rate of 0.15 $mL{\cdot}min^{-1}{\cdot}cm^{-2}$ was circulated. Finally, the current density applied was of 90 $mA{\cdot}cm^{-2}$. Fig. 10 illustrates the results obtained in terms of (a) concentration of formate and rate, and (b) Faradaic Efficiency and energy consumption as a function of the type of binder employed in the anode manufacture.

Despite the fact that similar values were reached in all the figures of merit represented in Fig. 10, it is important to remark that no degradation has been observed in Sustainion® anodes after the experiments. To confirm this observation, experiments with a duration of time of 5 h were tested at the same conditions defined previously. In this context, Fig. 11 represents the evolution of the formate concentration with time when using Nafion™ anodes or Sustainion® anodes.

The difference between both binders is quite substantial as seen in Fig. 11. The formate concentration achieved in the experiment with Nafion™ anodes decrease drastically after approximately one hour, obtaining negligible concentrations of the product after 2 h of continuous operation and no product output upon solely 3 h operation. In contrast, the formate concentration obtained with Sustainion® anodes remains stable along the 5 h of the experiment, representing a decrease of less than 13 % in the concentration, and therefore fulfilling one of the requirements for future implementation of this type of anodes in the electrochemical reduction of CO_2 to formate process. This issue could be attributed to the fact that the Sustainion® anion exchange ionomer can establish a local high pH environment around the NiO-based catalyst, promoting the OER in alkaline medium. Typically, Ni based catalysts are not stable at pH< 9 and many degradation mechanisms are triggered such as dissolution and redisposition of the nanoparticles at the membrane or even their detachment from the support towards the liquid electrolyte, limiting the OER activity of the catalyst and overall efficiency of the device. Besides, the low stability of Nafion™ anodes may occur since radicals produced during the oxygen evolution reaction in the anode directly destroy the structure of the Nafion™ ionomer, reacting with hydroxyls groups to generate compounds that destroy the function and integrity of the Nafion™ ionomer, based on perfluorosulfonic acid [78]. In this regard, the use of Sustainion® as binder at the anodes proved to be beneficial for boosting the efficiency of the reactor and should be considered for future industrial applications of CO_2 electrocatalytic reduction to formate.

3.6. Comparison with previous approaches using DSA/O2

Finally, in this subsection, the performance of the CO_2 electroreduction to formate process using Ni-based particulate electrodes is compared with respect to the results employing a DSA/O_2 as an anode using the same filter press reactor configuration and the same operating conditions. The comparison was carried out at an anolyte concentration of 1 M, an anolyte flow per geometric surface area of

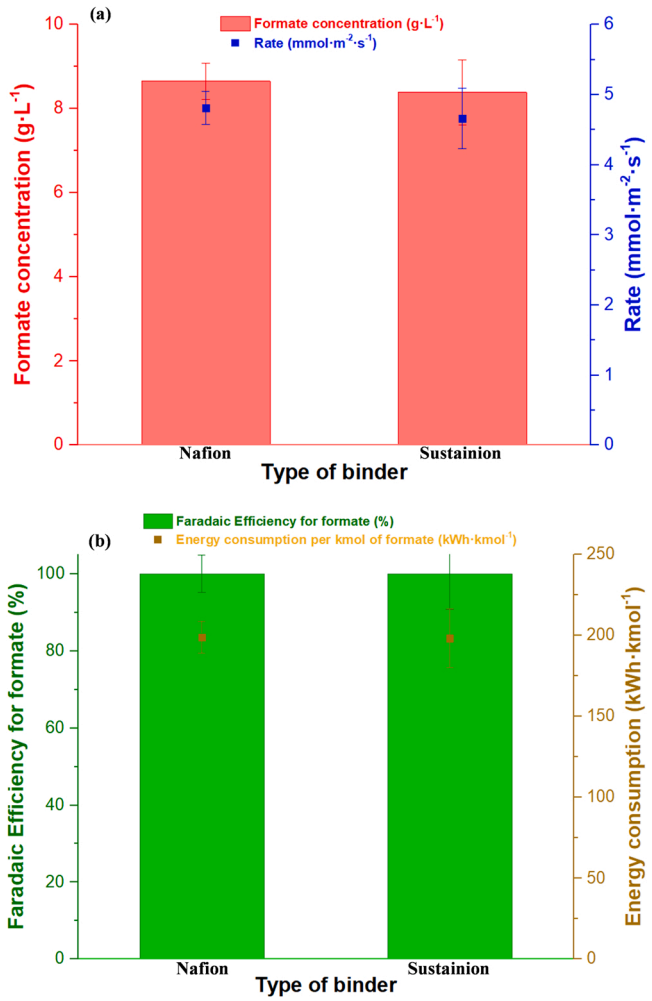

Fig. 10. Influence of the binder employed on the anode fabrication on (a) formate concentration ($g{\cdot}L^{-1}$) and rate ($mmol{\cdot}m^{-2}{\cdot}s^{-1}$) and (b) the Faradaic Efficiency for formate (%) and energy consumption per kmol of formate ($kWh{\cdot}kmol^{-1}$), at a current density = 90 $mA{\cdot}cm^{-2}$, a catholyte flow per geometric surface area = 0.15 $mL{\cdot}min^{-1}{\cdot}cm^{-2}$, a NiO catalyst loading = 1.5 $mg{\cdot}cm^{-2}$, a Bi catalyst loading = 0.75 $mg{\cdot}cm^{-2}$, an anolyte concentration = 1 M, and an anolyte flow = 11.4 $mL{\cdot}min^{-1}$.

1.14 $mL{\cdot}min^{-1}{\cdot}cm^{-2}$ and a NiO catalyst loading of 1.5 $mg{\cdot}cm^{-2}$, which allow for reaching the best results in previous subsections. Table 5 compares the main results achieved in this work using both types of binders with those obtained using DSA/O_2 with the same electrochemical reactor configuration.

Regardless of the binder used for the manufacture of the Ni-based particulate electrode, these anodes enhanced the performance of the CO_2 electroreduction to formate process in terms of formate concentration, Faradaic Efficiency, and product rate, in spite of obtaining slight increases of energy consumption of only 7 %. Firstly, the concentration of formate varied from 7.5 to approximately 8.4 or 8.6 $g{\cdot}L^{-1}$ increasing by approximately 15 %, a similar percentage as the formate rate. In this way, it is important to highlight the selectivities of formate achieved in this work (close to 100 %), demonstrating the feasibility and considerable potential of these anodes to carry out the OER and their coupling with the CO_2 electroreduction to formate in the cathode of the filter-press reactor. Thus, these anodes and particularly, NiO electrocatalysts can be considered as interesting materials to be used for the electrocatalytic reduction of CO_2 to value-added products.

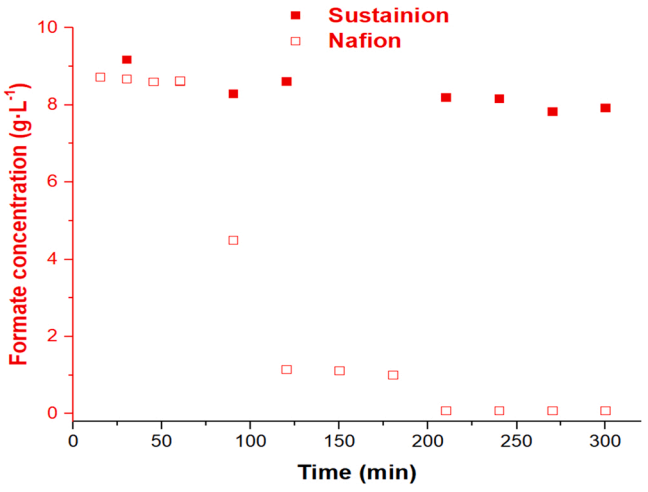

Fig. 11. Evolution of the formate concentration ($g{\cdot}L^{-1}$) with time (min) as a function of the kind of binder employed in the anode fabrication, at a current density = 90 $mA{\cdot}cm^{-2}$, a catholyte flow per geometric surface area = 0.15 $mL{\cdot}min^{-1}{\cdot}cm^{-2}$, a NiO catalyst loading = 1.5 $mg{\cdot}cm^{-2}$, a Bi catalyst loading = 0.75 $mg{\cdot}cm^{-2}$, an anolyte concentration = 1 M, and an anolyte flow = 11.4 $mL{\cdot}min^{-1}$.

4. Conclusions

In this work, Ni-based particulate anodes are assessed for the CO_2 electroreduction towards formate in a continuous filter press reactor with a single pass of the reactants through the electrochemical reactor. In this sense, these materials are used to catalyze the OER and to propose a real and competitive solution to substitute the traditional expensive and not-abundant materials, like Ir, Ti or Pt, typically used previously in the CO_2 electroreduction. Firstly, in this manuscript an electrochemical characterization of diverse NiO materials is carried out in a Rotative Disk Electrode by CV, LSV, and EIS techniques. This characterization demonstrates that NiO catalysts, with an average size of 50 nm, are an interesting material to carry out the OER, achieving promising results in terms of mass activity, geometric activity, and Tafel slopes in comparison with other Ni-based materials used in the literature. These materials are tested in a continuous CO_2 electrolyzer, studying firstly the influence of key variables in the process: (i) the current density (45, 90, 150 and 200 $mA{\cdot}cm^{-2}$), and (ii) the catholyte flow per geometric surface area (0.07, 0.15, and 0.57 $mL{\cdot}min^{-1}{\cdot}cm^{-2}$). In these experiments, anolyte concentration, and anolyte flow per geometric surface area were 1 M, and 0.57 $mL{\cdot}min^{-1}{\cdot}cm^{-2}$, respectively, the same as in previous recent studies with a DSA/O_2, with NiO catalyst loading of 0.75 $mg{\cdot}cm^{-2}$. In general, comparing these results under the same operating conditions, the figures of merit are close to, and even better than, those obtained previously. The concentrations achieved working with 200 $mA{\cdot}cm^{-2}$, and 0.15 $mL{\cdot}min^{-1}{\cdot}cm^{-2}$, of up to 13.42 $g{\cdot}L^{-1}$, with excellent values of Faradaic Efficiencies for formate and rate of 71.5 %, and 7.1 $mmol{\cdot}m^{-2}{\cdot}s^{-1}$, respectively, can be highlighted. Consequently, the effect of the NiO catalyst loading (0.75, 1.5, 2.25, and 3 $mg{\cdot}cm^{-2}$), the anolyte concentration (0.5, 0.75, 1, 1.5, and 2 M), and the anolyte flow per geometric surface area (0.57, 1.14, 1.71 and 2.28 $mL{\cdot}min^{-1}{\cdot}cm^{-2}$) was studied at a current density of 90 $mA{\cdot}cm^{-2}$ and a catholyte flow rate per geometric surface area of 0.15 $mL{\cdot}min^{-1}{\cdot}cm^{-2}$ using the same experimental setup as previous approaches developed in the research group to make a rigorous comparison.

In this sense, competitive results are obtained in terms of formate concentration (8.6 $g{\cdot}L^{-1}$), rate (4.8 $mmol{\cdot}m^{-2}{\cdot}s^{-1}$), and energy consumptions of only 200 $kWh{\cdot}kmol^{-1}$ with Faradaic Efficiency values for formate of approximately 100 %, enhancing the results reported in previous studies with a DSA/O_2. On the other hand, this study revealed that the durability of the anodes can be dramatically affected by the type

Table 5
Comparison of the results obtained with the Ni-based particulate electrode as a function of the type of binder employed for the manufacture of the anode with the previous results obtained using DSA/O_2 for a value of current density of 90 mA·cm^{-2}, catholyte flow per geometric surface area of 0.15 mL·min^{-1}·cm^{-2} at a Bi and NiO catalyst loading of 0.75 and 1.5 mg·cm^{-2}, respectively.

Type of counter electrode	Formate concentration (g·L^{-1})	Faradaic Efficiency (%)	Rate (mmol·m^{-2}·s^{-1})	Energy consumption (kWh·kmol^{-1})	Absolute cell potential (V)	Standard deviation (%)	Reference
Ni-based particulate electrode (Nafion™)	8.6	~100	4.8	199	3.8	3.5	This work
Ni-based particulate electrode (Sustainion®)	8.4	~100	4.7	198	3.6	4.9	This work
DSA/O_2	7.5	89.5	4.2	186	3.1	6.5	[68]

of binder used in the fabrication of the counter electrode. In this way, employing Sustainion® greatly enhances the durability of the anode with experiments with a duration times of at least 5 h, keeping similar results as those obtained previously with Ni-based particulate electrodes with Nafion™, and representing a decrease of less than 13 % in the formate concentration. Thus, the results here reported represent a step forward in the field of CO_2 electroreduction to formate due to the acquirement of competitive and promising values of key metrics in a continuous filter press reactor, using cheaper and more abundant materials as anodes, and therefore bringing this process closer for future implementation at the industrial scale.

CRediT authorship contribution statement

Guillermo Díaz-Sainz: Conceptualization, Methodology, Validation, Investigation, Data curation, Writing – original draft, Writing – review & editing. **Kevin Fernández-Caso:** Methodology, Validation, Investigation, Data curation. **Tiago Lagarteira:** Methodology, Validation, Investigation, Data curation, Writing – original draft. **Sofia Delgado:** Methodology, Validation, Investigation, Data curation, Writing – original draft. **Manuel Alvarez-Guerra:** Conceptualization, Writing – review & editing, Supervision, Project administration, Funding acquisition. **Adélio Mendes:** Writing – review & editing, Supervision, Project administration, Funding acquisition. **Angel Irabien:** Writing – review & editing, Supervision, Project administration, Funding acquisition.

Declaration of Competing Interest

The authors declare that they have no known competing financial interests or personal relationships that could have appeared to influence the work reported in this paper.

Data Availability

Data will be made available on request.

Acknowledgments

Authors fully acknowledge the financial support received from the Spanish State Research Agency (AEI) through the projects PID2019-108136RB-C31 and PID2020-112845RB-I00 (AEI/10.13039/501100011033). We are also grateful for the Bi carbon-supported nanoparticles prepared and provided by the group of Prof. V. Montiel and Dr. José Solla-Gullón from the Institute of Electrochemistry of the University of Alicante. Guillermo Díaz-Sainz would like to thank the Academic Planning and Teaching Staff Vice-chancellorship of University de Cantabria and the Young Chemical Researchers Group, belonging to the Royal Spanish Society of Chemistry (JIQ-RSEQ) for financial help to carry out the research stay at the Faculty of Engineering of the University of Porto in which the present work was developed.

Appendix A. Supporting information

Supplementary data associated with this article can be found in the online version at doi:10.1016/j.jece.2022.109171.

References

[1] More bad news for the planet: greenhouse gas levels hit new highs, World Meteorological Organization. https://public.wmo.int/en/media/press-release/more-bad-news-planet-greenhouse-gas-levels-hit-new-highs, 2022 (Accessed 7 December 2022).
[2] COP27 Sharm El-Sheikh Egypt 2022. https://cop27.eg/#/, 2022 (Accessed 7 December 2022).
[3] M. Mandal, CO_2 Electroreduction to Multicarbon Products, ChemElectroChem 7 (2020) 3713–3715, https://doi.org/10.1002/celc.202000798.
[4] P.R. Yaashikaa, P. Senthil Kumar, S.J. Varjani, A. Saravanan, A review on photochemical, biochemical and electrochemical transformation of CO_2 into value-added products, J. CO_2 Util. 33 (2019) 131–147, https://doi.org/10.1016/j.jcou.2019.05.017.
[5] W. Zhang, Y. Hu, L. Ma, G. Zhu, Y. Wang, X. Xue, R. Chen, S. Yang, Z. Jin, Progress and perspective of electrocatalytic CO_2 reduction for renewable carbonaceous fuels and chemicals, Adv. Sci. 5 (2018) 1700275, https://doi.org/10.1002/advs.201700275.
[6] S.A. Al-Tamreh, M.H. Ibrahim, M.H. El-Naas, J. Vaes, D. Pant, A. Benamor, A. Amhamed, Electroreduction of carbon dioxide into formate: a comprehensive review, ChemElectroChem 8 (2021) 3207–3220, https://doi.org/10.1002/celc.202100438.
[7] A. Irabien, M. Alvarez-Guerra, J. Albo, A. Domínguez-Ramos, Electrochemical conversion of CO_2 to value-added products, in: C.A. Martínez-Huitle, M.A. Rodrigo, O. Scialdone (Eds.), Electrochemical Water Wastewater Treat,emt, Elsevier, 2019, pp. 29–59.
[8] I. Merino-Garcia, L. Tinat, J. Albo, M. Alvarez-Guerra, A. Irabien, O. Durupthy, V. Vivier, C.M. Sánchez-Sánchez, Continuous electroconversion of CO_2 into formate using 2 nm tin oxide nanoparticles, Appl. Catal. B: Environ. 297 (2021), 120447, https://doi.org/10.1016/j.apcatb.2021.120447.
[9] D. Du, R. Lan, J. Humphreys, S. Tao, Progress in inorganic cathode catalysts for electrochemical conversion of carbon dioxide into formate or formic acid, J. Appl. Electrochem. 47 (2017) 661–678, https://doi.org/10.1007/s10800-017-1078-x.
[10] S. Zhao, S. Li, T. Guo, S. Zhang, J. Wang, Y. Wu, Y. Chen, Advances in Sn-Based catalysts for electrochemical CO_2 reduction, Nano-Micro Lett. 11 (2019) 62, https://doi.org/10.1007/s40820-019-0293-x.
[11] P. Ding, J. Zhang, N. Han, Y. Zhou, L. Jia, Y. Li, Simultaneous power generation and CO_2 valorization by aqueous Al-CO_2 batteries using nanostructured Bi_2S_3, Cathode Electro, J. Mater. Chem. A 8 (2020) 12385–12390, https://doi.org/10.1039/d0ta03761c.
[12] M.F. Philips, G.J.M. Gruter, M.T.M. Koper, K.J.P. Schouten, Optimizing the electrochemical reduction of CO_2 to formate: a state-of-the-art analysis, ACS Sustain. Chem. Eng. 8 (2020) 15430–15444, https://doi.org/10.1021/acssuschemeng.0c05215.
[13] I. Merino-Garcia, E. Alvarez-Guerra, J. Albo, A. Irabien, Electrochemical membrane reactors for the utilisation of carbon dioxide, Chem. Eng. J. 305 (2016) 104–120, https://doi.org/10.1016/j.cej.2016.05.032.
[14] H. Rabiee, L. Ge, X. Zhang, S. Hu, M. Li, Z. Yuan, Gas diffusion electrodes (GDEs) for electrochemical reduction of carbon dioxide, carbon monoxide, and dinitrogen to value-added products: a review, Energy Environ. Sci. 14 (2021) 1959–2008, https://doi.org/10.1039/d0ee03756g.
[15] R. Aldaco, I. Butnar, M. Margallo, J. Laso, M. Rumayor, A. Dominguez-Ramos, A. Irabien, P.E. Dodds, Bringing value to the chemical industry from capture, storage and use of CO_2: a dynamic LCA of formic acid production, Sci. Total Environ. 663 (2019) 738–753, https://doi.org/10.1016/j.scitotenv.2019.01.395.
[16] M. Rumayor, A. Dominguez-Ramos, A. Irabien, Environmental and economic assessment of the formic acid electrochemical manufacture using carbon dioxide: Influence of the electrode lifetime, Sustain. Prod. Consum 18 (2019) 72–82, https://doi.org/10.1016/j.spc.2018.12.002.

[17] M. Jouny, W. Luc, F. Jiao, General techno-economic analysis of CO_2 electrolysis systems, Ind. Eng. Chem. Res. 57 (2018) 2165–2177, https://doi.org/10.1021/acs.iecr.7b03514.
[18] X. Wang, F. Li, W.-J. Yin, Y. Si, M. Miao, X. Wang, Y. Fu, Atomically dispersed Sn modified with trace sulfur species derived from organosulfide complex for electroreduction of CO_2, Appl. Catal. B Environ. 304 (2022), 120936, https://doi.org/10.1016/j.apcatb.2021.120936.
[19] J. Li, J. Jiao, H. Zhang, P. Zhu, H. Ma, C. Chen, H. Xiao, Q. Lu, Two-dimensional SnO_2 nanosheets for efficient carbon dioxide electroreduction to formate, ACS Sustain. Chem. Eng. 8 (2020) 4975–4982, https://doi.org/10.1021/acssuschemeng.0c01070.
[20] A. Del Castillo, M. Alvarez-Guerra, J. Solla-Gullón, A. Sáez, V. Montiel, A. Irabien, Sn nanoparticles on gas diffusion electrodes: synthesis, characterization and use for continuous CO_2 electroreduction to formate, J. CO_2 Util. 18 (2017) 222–228, https://doi.org/10.1016/j.jcou.2017.01.021.
[21] H. Yang, J.J. Kaczur, S.D. Sajjad, R.I. Masel, Electrochemical conversion of CO_2 to formic acid utilizing Sustainion™ membranes, J. CO_2 Util. 20 (2017) 208–217, https://doi.org/10.1016/j.jcou.2017.04.011.
[22] C. Xia, P. Zhu, Q. Jiang, Y. Pan, W. Liang, E. Stavitsk, Continuous production of pure liquid fuel solutions via electrocatalytic CO_2 reduction using solid-electrolyte devices, Nat. Energy 4 (2019) 776–785, https://doi.org/10.1038/s41560-019-0451-x.
[23] L. Li, A. Ozden, S. Guo, F.P. García de Arquer, C. Wang, M. Zhang, J. Zhang, H. Jiang, W. Wang, H. Dong, D. Sinton, E.H. Sargent, M. Zhong, Stable, active CO_2 reduction to formate via redox-modulated stabilization of active sites, Nat. Commun. 12 (2021) 5223, https://doi.org/10.1038/s41467-021-25573-9.
[24] B. Ávila-Bolívar, L. García-Cruz, V. Montiel, J. Solla-Gullón, Electrochemical reduction of CO_2 to formate on easily prepared carbon-supported Bi nanoparticles, Molecules 24 (2019) 2032, https://doi.org/10.3390/molecules24112032.
[25] G. Díaz-Sainz, M. Alvarez-Guerra, A. Irabien, Continuous electroreduction of CO_2 towards formate in gas-phase operation at high current densities with an anion exchange membrane, J. CO_2 Util. 56 (2022), 101822, https://doi.org/10.1016/j.jcou.2021.101822.
[26] I. Grigioni, L.K. Sagar, Y.C. Li, G. Lee, Y. Yan, K. Bertens, R.K. Miao, X. Wang, J. Abed, D.H. Won, F.P. Garciá De Arquer, A.H. Ip, D. Sinton, E.H. Sargent, CO_2 electroreductionto formate at a partial current density of 930 mA cm^{-2} with InP colloidal quantum dot derived catalysts, ACS Energy Lett. (2020) 79–84, https://doi.org/10.1021/acsenergylett.0c02165.
[27] S.Z. Hou, X. Da Zhang, W.W. Yuan, Y.X. Li, Z.Y. Gu, Indium-based metal-organic framework for high-performance electroreduction of CO_2 to formate, Inorg. Chem. 59 (2020) 11298–11304, https://doi.org/10.1021/acs.inorgchem.0c00769.
[28] B. Ávila-Bolívar, V. Montiel, J. Solla-Gullón, On the activity and stability of Sb_2O_3/Sb nanoparticles for the electroreduction of CO_2 toward formate, J. Electroanal. Chem. 895 (2021), 115440, https://doi.org/10.1016/j.jelechem.2021.115440.
[29] J. García, C. Jiménez, F. Martínez, R. Camarillo, J. Rincón, Electrochemical reduction of CO_2 using Pb catalysts synthesized in supercritical medium, J. Catal. 367 (2018) 72–80, https://doi.org/10.1016/j.jcat.2018.08.017.
[30] Y. Kong, L. Wang, H. Jiang, F. Li, T. Zhao, M. Zhuo, Q. Chen, M. Mao, Y. Xu, Design of counter oxidation vs. CO_2 electroreduction for efficient formate production on a tin cathode, J. Electroanal. Chem. 847 (2019), 113264, https://doi.org/10.1016/j.jelechem.2019.113264.
[31] O. Scialdone, A. Galia, G. Lo Nero, F. Proietto, S. Sabatino, B. Schiavo, Electrochemical reduction of carbon dioxide to formic acid at a tin cathode in divided and undivided cells: Effect of carbon dioxide pressure and other operating parameters, Electrochim. Acta 199 (2016) 332–341, https://doi.org/10.1016/j.electacta.2016.02.079.
[32] F. Proietto, A. Galia, O. Scialdone, Electrochemical conversion of CO_2 to HCOOH at tin cathode: development of a theoretical model and comparison with experimental results, ChemElectroChem 6 (2019) 162–172, https://doi.org/10.1002/celc.201801067.
[33] B. De Mot, J. Hereijgers, M. Duarte, T. Breugelmans, Influence of flow and pressure distribution inside a gas diffusion electrode on the performance of a flow-by CO_2 electrolyzer, Chem. Eng. J. 378 (2019), 122224, https://doi.org/10.1016/j.cej.2019.122224.
[34] G. Díaz-Sainz, M. Alvarez-Guerra, B. Ávila-Bolívar, J. Solla-Gullón, V. Montiel, A. Irabien, Improving trade-offs in the figures of merit of gas-phase single-pass continuous CO_2 electrocatalytic reduction to formate, Chem. Eng. J. 405 (2021), 126965, https://doi.org/10.1016/j.cej.2020.126965.
[35] D. Li, L. Huang, T. Liu, J. Liu, L. Zhen, J. Wu, Y. Feng, Electrochemical reduction of carbon dioxide to formate via nano-prism assembled CuO microspheres, Chemosphere 237 (2019), 124527, https://doi.org/10.1016/j.chemosphere.2019.124527.
[36] W. Lee, Y.E. Kim, M.H. Youn, S.K. Jeong, K.T. Park, Catholyte-free electrocatalytic CO_2 reduction to formate, Angew. Chem. - Int. Ed. 57 (2018) 6883–6887, https://doi.org/10.1002/anie.201803501.
[37] G. Díaz-Sainz, M. Alvarez-Guerra, J. Solla-Gullón, L. García-Cruz, V. Montiel, A. Irabien, Catalyst coated membrane electrodes for the gas phase CO_2 electroreduction to formate, Catal. Today 346 (2020) 58–64, https://doi.org/10.1016/j.cattod.2018.11.073.
[38] G. Díaz-Sainz, M. Alvarez-Guerra, J. Solla-Gullón, L. García-Cruz, V. Montiel, A. Irabien, Gas–liquid–solid reaction system for CO_2 electroreduction to formate without using supporting electrolyte, AIChE J. 66 (2020), e16299, https://doi.org/10.1002/aic.16299.
[39] M. Fan, S. Prabhudev, S. Garbarino, J. Qiao, G.A. Botton, D.A. Harrington, A. C. Tavares, D. Guay, Uncovering the nature of electroactive sites in nano architectured dendritic Bi for highly efficient CO_2 electroreduction to formate, Appl. Catal. B Environ. 274 (2020), 119031, https://doi.org/10.1016/j.apcatb.2020.119031.
[40] T. Lei, X. Zhang, J. Jung, Y. Cai, X. Hou, Q. Zhang, J. Qiao, Continuous electroreduction of carbon dioxide to formate on Tin nanoelectrode using alkaline membrane cell configuration in aqueous medium, Catal. Today 318 (2018) 32–38, https://doi.org/10.1016/j.cattod.2017.10.003.
[41] K. Natsui, H. Iwakawa, N. Ikemiya, K. Nakata, Y. Einaga, Stable and highly efficient electrochemical production of formic acid from carbon dioxide using diamond electrodes, Angew. Chem. - Int. Ed. 57 (2018) 2639–2643, https://doi.org/10.1002/anie.201712271.
[42] Q. Yang, Q. Wu, Y. Liu, S. Luo, X. Wu, X. Zhao, H. Zou, B. Long, W. Chen, Y. Liao, L. Li, P.K. Shen, L. Duan, Z. Quan, Novel Bi-Doped amorphous SnO_x nanoshells for efficient electrochemical CO_2 reduction into formate at low overpotentials, Adv. Mater. 32 (2020) 2002822, https://doi.org/10.1002/adma.202002822.
[43] M. Park, W. Shin, Long-term stable and selective conversion of carbon dioxide to formate using dental amalgam electrode, J. CO_2 Util. 45 (2021), 101435, https://doi.org/10.1016/j.jcou.2021.101435.
[44] W. Luc, C. Collins, S. Wang, H. Xin, K. He, Y. Kang, F. Jiao, Ag-sn bimetallic catalyst with a core-shell structure for CO_2 reduction, J. Am. Chem. Soc. 139 (2017) 1885–1893, https://doi.org/10.1021/jacs.6b10435.
[45] M. Plevová, J. Hnát, K. Bouzek, Electrocatalysts for the oxygen evolution reaction in alkaline and neutral media. A comparative review, J. Power Sources 507 (2021), 230072, https://doi.org/10.1016/j.jpowsour.2021.230072.
[46] D.D. Qin, Y. Tang, G. Ma, L. Qin, C.L. Tao, X. Zhang, Z. Tang, Molecular metal nanoclusters for ORR, HER and OER: achievements, opportunities and challenges, Int. J. Hydrog. Energy 46 (2021) 25771–25781, https://doi.org/10.1016/j.ijhydene.2021.05.096.
[47] M. Yu, E. Budiyanto, H. Tüysüz, Principles of water electrolysis and recent progress in Cobalt-, Nickel-, and iron-based oxides for the oxygen evolution reaction, Angew. Chem. - Int. Ed. 3 (2021), e202103824, https://doi.org/10.1002/anie.202103824.
[48] M.I. Jamesh, X. Sun, Recent progress on earth abundant electrocatalysts for oxygen evolution reaction (OER) in alkaline medium to achieve efficient water splitting – a review, J. Power Sources 400 (2018) 31–68, https://doi.org/10.1016/j.jpowsour.2018.07.125.
[49] Z.P. Wu, X.F. Lu, S.Q. Zang, X.W. Lou, Non-noble-metal-based electrocatalysts toward the oxygen evolution reaction, Adv. Funct. Mater. 30 (2020) 1910274, https://doi.org/10.1002/adfm.201910274.
[50] J. Zhao, J.J. Zhang, Z.Y. Li, X.H. Bu, Recent progress on NiFe-Based ELectrocatalysts for the Oxygen Evolution Reaction, Small 16 (2020) 2003916, https://doi.org/10.1002/smll.202003916.
[51] D.M. Sayed, G.A. El-Nagar, S.Y. Sayed, B.E. El-Anadouli, M.S. El-Deab, Activation/deactivation behavior of nano-NiO_x based anodes towards the OER: influence of temperature, Electrochim. Acta 276 (2018) 176–183, https://doi.org/10.1016/j.electacta.2018.04.175.
[52] Y. Chen, A. Vise, W.E. Klein, F.C. Cetinbas, D.J. Myers, W.A. Smith, W.A. Smith, W. A. Smith, T.G. Deutsch, K.C. Neyerlin, A. Robust, Scalable platform for the electrochemical conversion of CO_2 to formate: identifying pathways to higher energy efficiencies, ACS Energy Lett. 5 (2020) 1825–1833, https://doi.org/10.1021/acsenergylett.0c00860.
[53] B. De Mot, M. Ramdin, J. Hereijgers, T.J.H. Vlugt, T. Breugelmans, Direct water injection in catholyte-free zero-gap carbon dioxide electrolyzers, ChemElectroChem 7 (2020) 3839–3843, https://doi.org/10.1002/celc.202000961.
[54] D. Wu, J. Hao, Z. Song, X.Z. Fu, J.L. Luo, All roads lead to Rome: an energy-saving integrated electrocatalytic CO_2 reduction system for concurrent value-added formate production, Chem. Eng. J. 412 (2021), 127893, https://doi.org/10.1016/j.cej.2020.127893.
[55] T. Fan, W. Ma, M. Xie, H. Liu, J. Zhang, S. Yang, P. Huang, Y. Dong, Z. Chen, X. Yi, Achieving high current density for electrocatalytic reduction of CO_2 to formate on bismuth-based catalysts, Cell Rep. Phys. Sci. 2 (2021), 100353, https://doi.org/10.1016/j.xcrp.2021.100353.
[56] Z. Xing, X. Hu, X. Feng, Tuning the microenvironment in gas-diffusion electrodes enables high-rate CO_2 electrolysis to formate, ACS Energy Lett. 6 (2021) 1694–1702, https://doi.org/10.1021/acsenergylett.1c00612.
[57] J. Yang, X. Wang, Y. Qu, X. Wang, H. Huo, Q. Fan, J. Wang, L.M. Yang, Y. Wu, Bi-Based metal-organic framework derived leafy bismuth nanosheets for carbon dioxide electroreduction, Adv. Energy Mater. 10 (2020) 2001709, https://doi.org/10.1002/aenm.202001709.
[58] J. Zou, C.Y. Lee, G.G. Wallace, A non-noble metal catalyst-based electrolyzer for efficient CO_2-to-formate conversion, ACS Sustain. Chem. Eng. 9 (2021) 16394–16402, https://doi.org/10.1021/acssuschemeng.1c06295.
[59] M. Zhang, W. Wei, S. Zhou, D.D. Ma, A. Cao, X.T. Wu, Q.L. Zhu, Engineering a conductive network of atomically thin bismuthene with rich defects enables CO_2 reduction to formate with industry-compatible current densities and stability, Energy Environ. Sci. 14 (2021) 4998–5008, https://doi.org/10.1039/D1EE01495A.
[60] Z. Wang, Y. Zhou, C. Xia, W. Guo, B. You, B.Y. Xia, Efficient electroconversion of carbon dioxide to formate by a reconstructed amino-functionalized indium–organic framework electrocatalyst, Angew. Chem. - Int. Ed. 60 (2021) 19107–19112, https://doi.org/10.1002/anie.202107523.
[61] L.P. Chi, Z.Z. Niu, X.L. Zhang, P.P. Yang, J. Liao, F.Y. Gao, Z.Z. Wu, K. Bin Tang, M. R. Gao, Stabilizing indium sulfide for CO_2 electroreduction to formate at high rate by zinc incorporation, Nat. Commun. 12 (2021) 5835, https://doi.org/10.1038/S41467-021-26124-Y.

[62] A. Seifitokaldani, C.M. Gabardo, T. Burdyny, C.T. Dinh, J.P. Edwards, M.G. Kibria, O.S. Bushuyev, S.O. Kelley, D. Sinton, E.H. Sargent, Hydronium-induced switching between CO_2 electroreduction pathways, J. Am. Chem. Soc. 140 (2018) 3833–3837, https://doi.org/10.1021/jacs.7b13542.

[63] A. Löwe, M. Schmidt, F. Bienen, D. Kopljar, N. Wagner, E. Klemm, Optimizing reaction conditions and gas diffusion electrodes applied in the CO_2 reduction reaction to formate to reach current densities up to 1.8 A cm^{-2}, ACS Sustain. Chem. Eng. 9 (2021) 4213–4223, https://doi.org/10.1021/acssuschemeng.1c00199.

[64] A. Löwe, C. Rieg, T. Hierlemann, N. Salas, D. Kopljar, N. Wagner, E. Klemm, Influence of temperature on the performance of gas diffusion electrodes in the CO_2 reduction reaction, ChemElectroChem 6 (2019) 4497–4506, https://doi.org/10.1002/celc.201900872.

[65] S. Liu, C. Wang, J. Wu, B. Tian, Y. Sun, Y. Lv, Z. Mu, Y. Sun, X. Li, F. Wang, Y. Wang, L. Tang, P. Wang, Y. Li, M. Ding, Efficient CO_2 electroreduction with a monolayer Bi_2WO_6 through a metallic intermediate surface state, ACS Catal. 11 (2021) 12476–12484, https://doi.org/10.1021/acscatal.1c02495.

[66] M.A. Rodríguez-Olguin, C. Flox, R. Ponce-Pérez, R. Lipin, F. Ruiz-Zepeda, J. P. Winczewski, T. Kallio, M. Vandichel, J. Guerrero-Sánchez, J.G.E. Gardeniers, N. Takeuchi, A. Susarrey-Arce, Chlorine in NiO promotes electroreduction of CO_2 to formate, Appl. Mater. Today 28 (2022), 101528, https://doi.org/10.1016/j.apmt.2022.101528.

[67] C. Oloman, H. Li, Electrochemical processing of carbon dioxide, ChemSusChem 1 (2008) 385–391, https://doi.org/10.1002/cssc.200800015.

[68] G. Díaz-Sainz, M. Alvarez-Guerra, J. Solla-Gullón, L. García-Cruz, V. Montiel, A. Irabien, CO_2 electroreduction to formate: continuous single-pass operation in a filter-press reactor at high current densities using Bi gas diffusion electrodes, J. CO_2 Util. 34 (2019) 12–19, https://doi.org/10.1016/j.jcou.2019.05.035.

[69] D. Xiang, L. Yin, Well-dispersed and size-tuned bimetallic PtFe x nanoparticle catalysts supported on ordered mesoporous carbon for enhanced electrocatalytic activity in direct methanol fuel cells, J. Mater. Chem. 22 (2012) 9584–9593, https://doi.org/10.1039/c2jm16641k.

[70] D.D. Zhu, J.L. Liu, S.Z. Qiao, Recent advances in inorganic heterogeneous electrocatalysts for reduction of carbon dioxide, Adv. Mater. 28 (2016) 3423–3452, https://doi.org/10.1002/adma.201504766.

[71] G.C. Anderson, B.S. Pivovar, S.M. Alia, Establishing performance baselines for the oxygen evolution reaction in alkaline electrolytes, J. Electrochem. Soc. 167 (2020), 044503, https://doi.org/10.1149/1945-7111/ab7090.

[72] F. Mori, M. Kubouchi, Y. Arao, Effect of graphite structures on the productivity and quality of few-layer graphene in liquid-phase exfoliation, J. Mater. Sci. 53 (2018) 12807–12815, https://doi.org/10.1007/S10853-018-2538-3.

[73] T. Lagarteira, S. Delgado, C. Fernandes, C. Azenha, C. Mateos-Pedrero, A. Mendes, The role of Pt loading on reduced graphene oxide support in the polyol synthesis of catalysts for oxygen reduction reaction, Int. J. Hydrog. Energy 45 (2020) 20594–20604, https://doi.org/10.1016/j.ijhydene.2020.02.022.

[74] Z. Liu, H. Yang, R. Kutz, R.I. Masel, CO_2 Electrolysisto CO and O_2 at high selectivity, stability and efficiency using sustainion membranes, J. Electrochem. Soc. 165 (2018) J3371–J3377, https://doi.org/10.1149/2.0501815jes.

[75] U.O. Nwabara, A.D. Hernandez, D.A. Henckel, X. Chen, E.R. Cofell, M.P. De-Heer, S. Verma, A.A. Gewirth, P.J.A. Kenis, Binder-focused approaches to improve the stability of cathodes for CO_2 electroreduction, ACS Appl. Energy Mater. 4 (2021) 5175–5186, https://doi.org/10.1021/acsaem.1c00715.

[76] I. Vincent, D. Bessarabov, Low cost hydrogen production by anion exchange membrane electrolysis: a review, Renew. Sustain. Energy Rev. 81 (2018) 1690–1704, https://doi.org/10.1016/j.rser.2017.05.258.

[77] B. Mayerhöfer, K. Ehelebe, F.D. Speck, M. Bierling, J. Bender, J.A. Kerres, K.J. J. Mayrhofer, S. Cherevko, R. Peach, S. Thiele, On the effect of anion exchange ionomer binders in bipolar electrode membrane interface water electrolysis, J. Mater. Chem. A 9 (2021) 14285–14295, https://doi.org/10.1039/D1TA00747E.

[78] M. Xie, T. Chu, T. Wang, K. Wan, D. Yang, B. Li, P. Ming, C. Zhang, Preparation, performance and challenges of catalyst layer for proton exchange membrane fuel cell, Membranes 11 (2021) 879, https://doi.org/10.3390/membranes11110879.